Defects improved photocatalytic ability of TiO$_2$

Lei Li[a], Hong-Wei Tian[a*], Fan-Ling Meng[a], Xiao-Ying Hu[b], Wei-Tao Zheng[a], and Chang Q Sun[c*]

[a] *Department of Materials Science and Key Laboratory of Automobile Materials of MOE and State Key Laboratory of Superhard Materials, Jilin University, Changchun 130012, China.*

[b] College of Science, Changchun University, Changchun 130022, China

[c] *School of Electrical and Electronic Engineering, Nanyang Technological University, Singapore 639798.*

Corresponding author, E-mail: Tianhw@jlu.edu.cn; ecqsun@ntu.edu.sg

1

2 **Abstract**

3

4 Defect generation forms an important means modulating the photocatalytic ability of TiO_2 with

5 mechanisms that remain yet unclear. Here we show that a spectral distillation clarifies the impact of

6 defect on modulating the band gap, electroaffinity, and work function of the substance. Firstly, by

7 analyzing XPS measurements, we calibrated the $2p_{3/2}$ level of 451.47 eV for an isolated Ti atom and

8 its shifts by 2.14 and 6.94 eV, respectively, upon Ti and TiO_2 bulk formation. Spectral difference

9 between the defected and the un-defected TiO_2 skin revealed then that the $2p_{3/2}$ level shifts further

10 from 6.94 to 9.67 eV due to the defect-induced quantum entrapment. This entrapment is associated

11 with an elevation of the upper edges of both the $2p_{3/2}$ and the conduction band by polarization. The

12 shortening and strengthening of bonds between undercoordinated atoms densify and entrap the core

13 electrons, which in turn polarize the dangling bond electrons of defect atoms. The entrapment and

14 polarization mediate thus the band gap, the electroaffinity, the work function, and the photocatalytic

15 ability of TiO_2.

16

17

18 Key Words: Photocatalysis, XPS, DFT, TiO_2, defect, surface, nanostructures

1   Introduction

Defects are ubiquitous but generally undesired in applications, as they introduce unpredictability and difficulty in understanding. However, if properly controlled, they can form the base of a completely new technology that issue sustainable, scalable applications as a cheap and convenient method. Atomic undercoordination, such as situations of adatoms, atomic defects, terrace edges, monolayer skin of the bulk, and nanostructures, alters the local bond and electronic attributes, including the bond length, bond energy, potential trap depth, charge and energy density [1], electroaffinity, band gap, and work function in terms of entrapment and polarization [2]. These entities determine the performance of a substance at the specific atomic site, such as the catalytic ability, electronic, dielectric, optic, magnetic, mechanical, and thermal properties. Thus, an atomic-scale understanding of the energetic behavior of electrons due to defect becomes increasingly important in systems with a large number of such undercoordinated atoms.

The photoactivity of the nanoscaled or the highly-defected TiO_2 has received extensive attention owing to its tunable band gap and work function [3-8]. The drawbacks of bulk TiO_2 stem from its wide band gap and massive photogenerated charge carriers prevent carriers from being generated under visible-light irradiation and from living longer by postponed recombination [9, 10]. Much effort has been made to improve the photovoltaic or photocatalytic ability of TiO_2 by introducing defects in past decades. Although the defected-TiO_2 containing Ti^{3+} ions and O^{2-} vacancies could absorb visible light [11, 12], the mechanism of band structure modulation remains inconclusive.

It has been elegantly accepted that the oxygen-derived Ti 3d states located ~0.85 eV below the Fermi level (E_F) narrows the band gap [9, 13]. Such Ti 3d states are conventionally ascribed to the oxygen (O_{br}) vacancies in bridging two Ti^{3+} ions across [14-16]. Each O_{br} vacancy may leave two electrons behind the neighboring Ti atoms during vacating. However, based on their ultra-violet spectroscopy (UPS), scanning tunneling microscopy (STM), and density functional theory (DFT) investigation, Mattinez et al [3] suggested that the Ti 3d defect states at the $TiO_2(110)$ surface arise primarily from Ti^{3+} interstitials in the near-surface region rather than to the surface O_{br} vacancies. The defected black TiO_2 exhibits substantial activity and stability in the photocatalytic production of hydrogen

from water under sunlight [17]. Combining valence band x-ray photoelectron spectroscopy (XPS) and optical absorption spectroscopy, they found that not only the valence band but also the center of the conduction band of the black TiO_2 shifts up simultaneously. Therefore, band bending due to defects play important roles in photocatalysis and photochemical processes of TiO_2 [18].

In this communication, we show that a combination of the zone-selective electronic spectroscopic (ZPS) analysis [19] and the bond order-length-strength and nonbonding electron polarization (BOLS-NEP) notation [2, 20] have enabled us to purify and quantify the defect states with clarification of their physical origin.

2   Principles

2.1   Core level shift: Tight-binding approach

According to the tight-binding (TB) theory [21], the integral of the intra-atomic potential, $V_{atom}(r)$, and the respective electronic eigen wave function at the specific ith atomic site, $|v,i\rangle$, determines the vth energy level of an isolated atom, $E_v(z = 0)$. The involvement of the interatomic potential $V_{cry}(r)$ shifts the $E_v(0)$ to a deeper energy by an amount that is proportional to the cohesive energy per bond at equilibrium, which follows [21],

$$H = -\frac{\hbar^2 \nabla^2}{2m} + V_{atom}(r) + V_{cry}(r)$$

$$E_v(0) = \langle v,i|V_{atom}(r)|v,i\rangle$$

$$E_v(12) - E_v(0) = \langle v,i|V_{cry}(r)|v,i\rangle + \sum_{j=1}^{j=z}\langle v,i|V_{cry}(r)|v,j\rangle$$

$$= \alpha\left(1 + \frac{z\beta}{\alpha}\right) \cong \alpha \propto E_b$$

(1)

The coordination number (CN) $z = 0$ represents an isolated atom and $z_b = 12$ an atom in the fcc bulk as standard reference. The sum is over all z neighbors of the specific ith atom. The parameter α is the exchange integral and the β the overlap integral. Because $\langle v,i|v,j\rangle = \delta_{ij}$ with δ_{ij} being the Kronig function (if $i = j$, $\delta_{ij} = 1$, otherwise, $\delta_{ij} = 0$), the term $z\beta/\alpha << 1$, the β is negligible compared with the α. Any perturbation to the bond energy E_b will shift the core level accordingly.

2.2 BOLS-NEP: Quantum entrapment and polarization

The BOLS-NEP notation [2] indicates that atomic undercoordination shortens and strengthens the remaining bonds between undercoordinated atoms. Bond contraction raises the local density of the bonding charge, energy, and mass; bond strengthening deepens the local potential well and entraps the electrons with deeper binding energy [1].

On the other hand, the locally densely entrapped core and bonding electrons will polarize the nonbonding (dangling bond in the present case) electrons and raise their energy close to the Fermi energy or cross. The polarized electrons in turn will split and screen the local potentials, which create polarized states to the core band unless the core band is too deep to be sensitive to the polarization perturbation. These sequential BOLS-NEP events perturb the Hamiltonian of an extended solid. Figure 1 illustrates the BOLS-NEP scheme on the behavior of bonding and nonbonding electrons at sites of undercoordinated atoms. These sequential processes modulate the gap between the conduction and the valence band, electroaffinity or separation between the vacuum level and the bottom edge of the conduction band, work function and tune the photocatalytic ability of the defected-TiO_2. The deepening of the conduction band and the polarization of the valence band narrow the band gap for photon absorption; the polarization of the conduction band reduces the work function for electron rejection; and the entrapment of the conduction band enlarges the electroaffinity that represents the ability of holding electrons from being escaped or recombined.
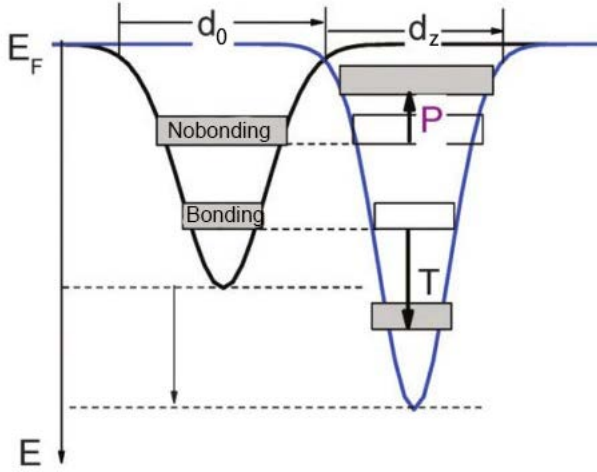
Figure 1 BOLS-NEP notation indicates that atomic undercoordination shortens the local bond ($d_z <$ d_0) and deepens the local potential well that densifies and entraps the bonding electrons (T). The densely entrapped electrons polarize the nonbonding electrons to form the polarized states (P) shifting up. The polarized states will screen and split the local potential, which will add polarized states to the core band unless the core band is too deep to be sensitive to the polarization.

The polarized electrons neither follow the standard dispersion nor occupy the allowed states defined by the Hamiltonian; instead, they generate states in the vicinity of Fermi energy. These electrons are responsible for the size emergence of nanostructures such as the dilute magnetism, catalytic enhancement, Dirac-Fermions for topological insulators, etc. [22, 23].

Defect formation perturbs the crystal potential in the Hamiltonian with an addition of Δ_H:

$$H' = -\frac{\hbar^2 \nabla^2}{2m} + V_{atom}(r) + V_{cry}(r)[1 + \Delta_H]$$

Where

$$1 + \Delta_H = \begin{cases} C_z^{-m} = E_z/E_0 & \text{(Quantum entrapment)} \\ p = [E_v(P) - E_v(0)]/[E_v(12) - E_v(0)] & \text{(Polarization)} \end{cases}$$

$$C_z = d_z/d_0 = 2/\{1 + exp[(12 - z)/(8z)]\} \quad \text{(Bond contraction coefficient)}$$

(2)

P is the polarization coefficient to be determined using photoelectron spectroscopy measurement. The $E_v(x)$ is the spectral peak energy with x representing the T and P components. C_z is the z-dependent bond contraction coefficient, which varies only with the effective atomic CN and has

nothing to do with the dimensionality or the structure phase. E_0 and d_0 are the bond energy and bond length of the bulk standard, respectively. The bond nature indicator m is an adjustable parameter that keeps constant for the same substance.

Incorporating the BOLS correlation into the TB approach yields the energy shift of the vth level of z-coordinated atom from that of the isolated atom:

$$\Delta E_v(z) = E_v(z) - E_v(0) = \Delta E_v(12)(1 + \Delta_H(z))$$

where

$$\begin{cases} \Delta E_v(z) = \alpha(z) + z\beta(z) \propto \langle E_z \rangle & \text{(Core level shift)} \\ \alpha = \langle v, i | V_{cry}(r)(1 + \Delta_H) | v, i \rangle \propto \langle E_z \rangle & \text{(Exchange integral)} \\ \beta = \langle v, i | V_{cry}(r)(1 + \Delta_H) | v, i' \rangle \propto \langle E_z \rangle & \text{(Overlap integral)} \end{cases}$$

$$(3)$$

The mean bond energy, $\langle E_z \rangle$, dominates the core level shift. Eq (3) yileds:

$$\frac{E_v(z) - E_v(0)}{E_v(12) - E_v(0)} = \frac{E_z}{E_{12}} = 1 + \Delta_H(z) = \begin{cases} C_z^{-m} & \text{(Entrapment)} \\ p + 1 & \text{(Polarization)} \end{cases}$$

$$(4)$$

The bond nature indicator m is to be optimized in decomposing the XPS spectrum. For situations without apparent polarization, the relation evolves,

$$\frac{E_v(z) - E_v(0)}{E_v(z') - E_v(0)} = \frac{C_{z'}^m}{C_z^m} \quad or \quad \frac{E_v(z) - E_v(12)}{E_v(z') - E_v(12)} = \frac{C_{z'}^m - 1}{C_z^m - 1} \quad (z \neq z')$$

$$(5)$$

which yields,

$$\begin{cases} E_v(0) = \dfrac{C_{z'}^{-m} E_v(z) - C_z^{-m} E_v(z')}{C_{z'}^{-m} - C_z^{-m}} = \dfrac{C_z^m E_v(z) - C_{z'}^m E_v(z')}{C_z^m - C_{z'}^m} \\ \Delta E_v(12) = [E_v(z) - E_v(0)] C_z^m \\ E_v(z) = \langle E_v(0) \rangle + \Delta E_v(12) C_z^{-m} \end{cases}$$

$$(6)$$

One can determine the energy level of an isolated atom and its z-dependent shift by decomposing XPS spectra using constraint of Eq (6) [24].

Based on the BOLS-NEP notation, we can also predict the z-resolved relative atomic cohesive energy ($E_c = E_c(z)/E_c(12) = z_z E_z/z_b E_b = z_{zb} C_z^{-m}$) and the local binding energy density ($E_d = [E_d(z)/d_z^3]/[E_d(12)/d_0^3] = C_z^{-(m+3)}$) at an atomic site. Therefore, one can obtain comprehensive information regarding the bond order, length, energy, atomic cohesive energy, and the binding energy density (z, d_z, E_z, E_c, and E_d) with or without polarization from XPS measurements. These quantities are of fundamental importance to understanding the properties and reaction dynamics pertaining to atoms with any number of neighbors.

2.3 ZPS: Density-of-states distillation

Zone-selective photoelectron spectroscopy (ZPS) [19] was invented to purify local and quantitative information on the bonding and electronic dynamics associated with the monolayer skin and atomic defects [25]. The residual spectrum of a ZPS is obtained by differencing two XPS spectra collected from (i) the same undefected surface at different emission angles and (ii) a surface after and before the surface being chemically or physically conditioned (such as defect generation and chemisorption) under the same measurement conditions. Upon background correction and spectral area normalization, the ZPS in (i) discriminates the spectral features of the monolayer skin with least CN from that of the bulk with highest atomic CN. The ZPS removes the commonly shared spectra area. An XPS collects more information from the surface at larger emission angles. Likewise, the ZPS in (ii) purifies merely the spectral features due to the conditioning.

In the present work, we subtracted the XPS and UPS spectrum of the undefected TiO_2 surface from that of the defected-TiO_2, the residual spectrum retains only the features due to the defect atoms. Especially, the ZPS removes all artifact backgrounds, such as the charging and the "initial–final states" relaxation effects that exist throughout the course of measurement.

2.4 The mechanism of TiO_2 photocatalysis

1 As the mostly used photocatalyst, TiO_2 has been extensively investigated since 1977 when Frank and

2 Bard [26] firstly proposed TiO_2 for decomposing cyanide. Figure 2 illustrates the principle for TiO_2

3 photocatalytic reaction. When a TiO_2 surface is illuminated by light with energy being equal to or

4 larger than the band gap energy, the radiation photons excite electrons in the ground valance band

5 (VB) to the upper conduction band (CB, e^-), leaving a hole (h^+) behind the VB. The excited charge

6 carriers (electrons and holes also called excitons) are highly reactive to radicals with robust reducing

7 and oxidizing capacity respectively that may recombine or get trapped in metastable surface states, or

8 react with suitable electron acceptors/donors pre-adsorbed on the catalyst surface.

9

10 Two entities are of concern to enhance the photocatalytic efficiency of TiO_2: i) light wavelengths

11 excavating electrons to surpass the band gap of TiO_2 in the UV range, which are only accounts for 4%

12 of solar light; ii) in the photocatalytic reaction, when the reduction and oxidation do not proceed

13 simultaneously, there is an electron accumulation in the CB, thereby causing a fast recombination of

14 the e-h pairs. Therefore, improve the utilization rate of sunlight by modulating band gap and raise

15 electrons lifetime by reducing the work function ($\boldsymbol{\Phi}$) via locally pinning the polarized electrons is
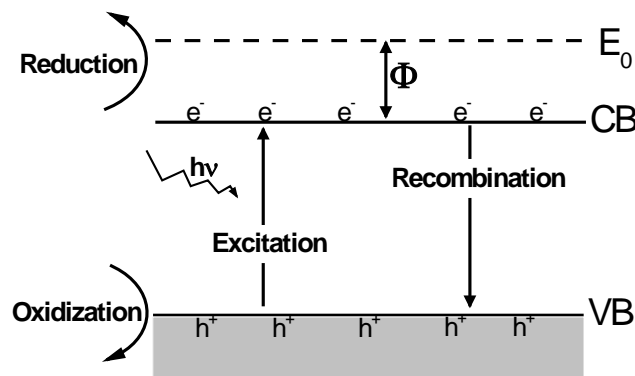
16 essential.

17

18 Figure 2 Schematic illustrations of electron transferring in the photocatalytic reaction. The incident

19 light produces e-h pairs that undergo thermalization and then recombination if the excited electrons

20 retain in the conduction band. The excited electrons reserve for catalytic activity. Therefore,

21 modulation of the band gap, electroaffinity (separation between the vacuum level and the bottom

1   edge of the CB), and work function (Φ) are of key factors controlling the photocatalytic behavior.

2

3   ## 3   Results and discussion

4

5   ### 3.1 Ti(0001): $E_{2p}(0)$ and $\Delta E_{2p}(12)$

6

7   In order to calibrate and quantify the electron binding-energy shift of the defected-TiO$_2$, we firstly

8   decomposed the XPS spectra from well-faceted Ti(0001) surface to obtain the energy level of an

9   isolated Ti atom and its bulk shift. Based on the BOLS-TB notation, we decomposed the Ti(0001)

10    $2p_{3/2}$ spectrum [27] into four components. These components are the bulk (B) and surfaces (S_i, i = 1,

11   2, 3) ordered as B, S_3, S_2 and S_1 from higher (closer the E_F) to lower binding energy (BE), as shown

12   in Figure 3.

13

14   The presently optimized atomic CN (z_1 = 3.50, z_2 = 4.36, z_3 = 6.48 and z_B = 12.00) is identical to

15   those derived from the same hcp surfaces of Be(0001) [24] and Ru(0001) [28]. The $E_v(0)$ and

16    $E_v(12)$ are intrinsic constants for a given material, regardless of their orientations or chemical

17   conditions. For simplicity, we refer the energy shift of all surface components to the $E_v(12)$ before

18   knowing the $E_v(0)$ value. There are a total of l = 4 components involved for the Ti (0001) surface

19   as shown in Figure 3. One can find the mean $< E_v(0) >$ from the C $=4!/(4-2)!2! = 6$ possible

20   values of $E_v(0)$ from eq (6),

21

22    $$\langle E_{2p_{3/2}}(0) \rangle = \sum_6 E_{2p_{3/2}}(0)/6 = 451.47 \text{eV},$$

23

24   with the standard deviation of:

25

26    $$\sigma = \left\{ \sum \left[E_{2p_{3/2}}(0) - \langle E_{2p_{3/2}}(0) \rangle \right]^2 /N/(N-1) \right\}^{1/2} = 0.003.$$

27

28   The $\Delta E_{2p_{3/2}}(12) = 2.14$ eV and the optimized $E_{2p_{3/2}}(12) = 453.61$ eV were thus obtained for the Ti

29   with the following expression for the layer-resolved core level shift:

1

$$E_{2p_{3/2}}(z) = \langle E_{2p_{3/2}}(0) \rangle + \left[E_{2p_{3/2}}(12) - E_{2p_{3/2}}(0) \right] C_z^{-m}$$

$$= 451.47 \pm 0.003 + 2.14 C_z^{-4.6}.$$

The refinement leads to the bond nature indicator m = 4.6 for Ti. Besides, with the derived z and m values, we elucidate the layer-resolved local strain ($C_z - 1$), relative binding energy density $\left(C_z^{-(m+3)} \right)$, and the relative atomic cohesive energy ($z_{zb} C_z^{-m}$) for each surface component, as featured in Table1.
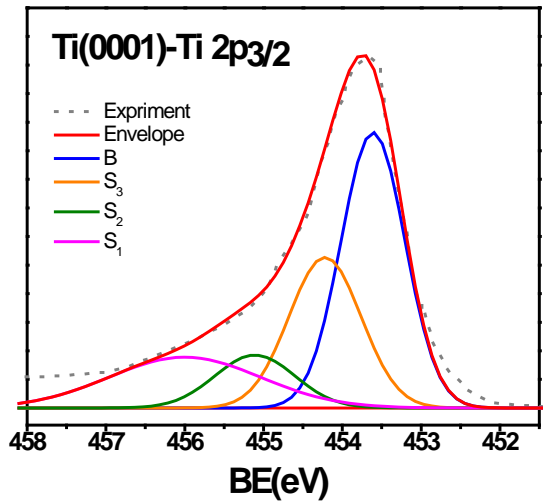
Figure 3 Decomposition of the Ti(0001) XPS spectrum with derived information featured in Table 1. The energy shift of each component is proportional to the bond energy, which follows this relation:

$$E_v(z)/E_v(12) = E_z/E_B = C_z^{-m}.$$

Table 1 Information of the effective CNs, bond length, bond energy, relative binding energy density, relative atomic cohesive energy and the layer-dependent core level shift for Ti(0001) surface with bond nature indicator m = 4.6.

	i	$E_{2p_{3/2}}$	z	d_z(Å)	E_z(eV)	$C_z - 1$	$C_z^{-(m+3)}$	$z_{zb} C_z^{-m}$

	atom	451.47	0	-	-	-	-	-
	B	453.61	12.00	2.934	0.4717	0.00	1.00	1.00
Ti(0001)	S_3	454.22	6.48	2.850	0.539	-5.32	1.51	0.69
	S_2	455.11	4.36	2.718	0.670	-10.91	2.41	0.61
	S_1	456.00	3.50	2.578	0.855	-15.06	3.63	0.61

3.2 ZPS of defected-TiO$_2$: Ti$_{2p3/2}$ and O$_{1s}$ core bands

The ZPS in Figure 4 shows the defect-induced Ti $2p_{3/2}$ and O1s states. The ZPS was obtained by subtracting the spectrum collected from a undefected TiO$_2$(110) surface as a reference from that of the defected-TiO$_2$(110) surface (defects were obtained by Ar$^+$ bombardment) after background correction and spectral peak area normalization [29]. The ZPS spectra revealed the following:

(i) The B valley at 458.41 eV in (a) corresponds to the Ti $2p_{3/2}$ bulk component and at 529.83 eV in (b) to the O1s in the bulk TiO$_2$. According to BOLS-NEP notation, for a surface with undercoordinated atoms, the bulk information is partially annihilated because of undercoordination-induced energy shift, therefore, the differential spectra show a valley, B. The interaction between Ti and O substantially magnifies the crystal potential, which results in the Ti $2p_{3/2}$ states shifting positively by 4.8 eV compared with that of the bulk Ti.

(ii) The defected Ti $2p_{3/2}$ shows both the entrapment (T = 461.14 eV) and the polarization states (P = 456.41 eV). The T is below and the P is above the B (458.41 eV), as we expected. However, the O1s shows only quantum entrapment (T = 531.33 eV) without presence of polarization. The 528.83-458.41 = 71.42 eV deeper of the innerest O 1s orbital is insensitive to the polarization effect compared to the Ti 2p orbital.

(iii) The extents of the entrapment and the polarization increase with the concentration of defects. According to Table 1, the effective CN of the defected-TiO$_2$ should be lower than the ideal surface of 3.5 for the Ti(0001) skin. The ZPS gives polarization coefficient as:

$$p = \left[E_{2p_{3/2}}(P) - E_{2p_{3/2}}(0)\right]/\left[E_{2p_{3/2}}(12\,(TiO_2)) - E_{2p_{3/2}}(0)\right] = 0.71.$$

Because the core level shift is proportional to the equilibrium bond energy, we can also obtain the TiO$_2$ bulk bond energy $\langle E_b(TiO_2)\rangle = 1.51$ ev/bond and defected bond energy $\langle E_b(\text{defect})\rangle = 2.11$ ev/bond in comparison to that of Ti bulk bond energy $\langle E_b(Ti)\rangle = 0.41$eV/bond [30].
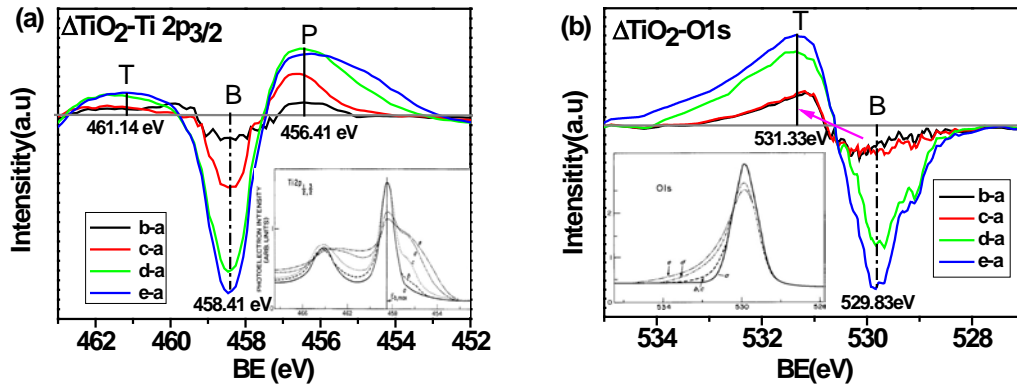

Figure 4 ZPS of (a) the Ti 2p$_{3/2}$ and (b) O1s of the defected TiO$_2$ with respect to the undefected TiO$_2$ under different defect concentrations. The insets show the raw XPS spectra sourced from [29]: a, undefected; b, thermally produced defects; Ar$^+$ bombardment for c, 10 min; d, 30 min; and e, 50 min. B, T, and P denote the bulk, entrapped, and polarized states. The absence of the P states of the O1s indicates that this innerest orbit is insensitive to the polarization.

3.3 ZPS of defected-TiO$_2$: Valence band

In order to elucidate the relationship between bond contraction and catalytic enhancement of defected-TiO$_2$, we also analyzed the ZPS of the VB when the TiO$_2$(110) surface is reduced by Ar$^+$ bombardment (Figure 5)[16]. Results also show the entrapped and the polarized features which are substantially the same as those observed from the *2p* core band of the defected-TiO$_2$. Therefore, the valence and the core electrons shift simultaneously in the same fashion because of the screening effect to the core charge, being the same to what happened to AgPd and CuPd alloy catalysts [31], and the Pt and Rh adatoms [2]. Work function is reduced by the locked dipoles other than free

electrons. The extent of localization and polarization increases with the drop of the atomic CN. Therefore, the life of the locked dipoles is relatively longer than the otherwise, which is beneficial to the catalytic ability of the defected TiO_2.
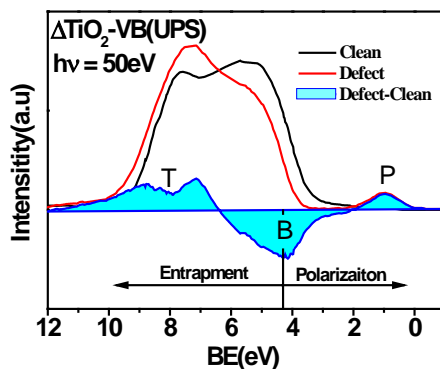

Figure 5 The valence ZPS of the defected-TiO_2 shows the presence of both the polarization (P) and the entrapment (T) attributes, being consistent to the core band shift. The presence of the P states lowers the work function by locked dipoles, which is beneficial to charge offering in catalytic reaction but prevent combination. The presence of the T states enlarges the electroaffinity, which stabilize electrons hindering combination.

4   Conclusion

A combination of the BOLS-NEP notation and the ZPS strategy has enabled us to identify the physical origin of the defect-enhanced catalytic ability of TiO_2. Atomic undercoordination shortens and strengthens the local bond with local densification, entrapment, and polarization of the valence and the conduction electrons, which revises the band structure. The entrapment deepens the bottom edges and polarization raises the upper edges of all the bands, which narrows the band gap, reduces the work function, and enlarges the electroaffinity of the substance. The reduced gap enables TiO_2 to respond to longer wavelength of sunlight for exciting electrons. The increased electroaffinity hinders electron-hole recombination and the lowered work function offers electrons easily in the process of catalysis. Therefore, mechanism for defects modulation to the catalytic ability of TiO_2 becomes clear, which can be extended to the understanding of other catalysts such as noble metals.

References

1. L. Wan, S. Xu, M. Liao, C. Liu, and P. Sheng, *Self-Consistent Approach to Global Charge Neutrality in Electrokinetics: A Surface Potential Trap Model.* Physical Review X **4**(2014) 011042.

2. C.Q. Sun, *Relaxation of the Chemical Bond*. Springer Series in Chemical Physics. Vol. 108. 2014 Berlin:Springer press; ISBN:978-981-4585-20-0. 550.

3. U. Martinez, J. Hansen, E. Lira, H. Kristoffersen, P. Huo, R. Bechstein, E. Lægsgaard, F. Besenbacher, B. Hammer, and S. Wendt, *Reduced step edges on rutile TiO$_2$(110) as competing defects to oxygen vacancies on the terraces and reactive sites for ethanol dissociation.* Physical Review Letters **109**(2012).

4. S. Jin, Y. Li, H. Xie, X. Chen, T. Tian, and X. Zhao, *Highly selective photocatalytic and sensing properties of 2D-ordered dome films of nano titania and nano Ag^{2+} doped titania.* Journal of Materials Chemistry **22**(2012) 1469.

5. A. Borodin and M. Reichling, *Characterizing TiO$_2$(110) surface states by their work function.* Physical Chemistry Chemical Physics **13**(2011) 15442-7.

6. C.M. Yim, C.L. Pang, and G. Thornton, *Oxygen vacancy origin of the surface band-gap state of TiO$_2$(110).* Physical Review Letters **104**(2010).

7. M. Kong, Y. Li, X. Chen, T. Tian, P. Fang, F. Zheng, and X. Zhao, *Tuning the relative concentration ratio of bulk defects to surface defects in TiO$_2$ nanocrystals leads to high photocatalytic efficiency.* Journal of the American Chemical Society **133**(2011) 16414-7.

8. J. Tao and M. Batzill, *Role of surface structure on the charge trapping inTiO$_2$ photocatalysts.* J. Phys. Chem. Lett. **1**(2010) 3200-3206.

9. U. Diebold, *The surface science of titanium dioxide* SURFACE SCIENCE REPORTS **48**(2003) 53-229.

10. R. Daghrir, P. Drogui, and D. Robert, *Modified TiO$_2$ for environmental photocatalytic applications: A review.* Industrial & Engineering Chemistry Research (2013) 130226090752004.

11. K. Kollbek, M. Sikora, C. Kapusta, J. Szlachetko, K. Zakrzewska, K. Kowalski, and M. Radecka5, *X-ray spectroscopic methods in the studies of nonstoichiometric TiO$_{2-x}$ thin films.* Applied Surface Science (2013).

12. F. Zuo, L. Wang, T. Wu, Z. Zhang, D. Borchardt, and P. Feng, *Self-doped Ti^{3+} enhanced photocatalyst for hydrogen production under visible light.* J. AM. CHEM. SOC **132**(2010) 11856–11857.

13. K. Mitsuhara, H. Okumura, A. Visikovskiy, M. Takizawa, and Y. Kido, *The source of the Ti 3d defect state in the band gap of rutile titania (110) surfaces.* The Journal of Chemical Physics **136**(2012) 124707.

14. S. Chrétien and H. Metiu, *Electronic structure of partially reduced rutile TiO$_2$(110) surface: Where are the unpaired electrons located?* The Journal of Physical Chemistry C **115**(2011) 4696-4705.

15. P. Krüger, S. Bourgeois, B. Domenichini, H. Magnan, D. Chandesris, P. Le Fèvre, A. Flank, J. Jupille, L. Floreano, A. Cossaro, A. Verdini, and A. Morgante, *Defect states at the TiO$_2$(110) surface probed by resonant photoelectron diffraction.* Physical Review Letters **100**(2008).

16. Z. Zhang, S.-P. Jeng, and V. Henrich, *Cation-ligand hybridization for stoichiometric and reduced TiO$_2$ (110) surfaces determined by resonant photoemission.* PHYSICAL REVIEW B **43**(1991) 12004-12011.

17. X. Chen, L. Liu, P.Y. Yu, and S.S. Mao, *Increasing solar absorption for photocatalysis with black hydrogenated titanium dioxide nanocrystals.* Science **331**(2011).

18. Z. Zhang and J.T. Yates, Jr., *Band bending in semiconductors: chemical and physical consequences at surfaces*

and interfaces. Chem Rev **112**(2012) 5520-5551.

19. C.Q. Sun, *Atomic scale purification of electron spectroscopic information (USA patent: publication: US20130090865)*, 18, June 2010: USA.

20. Y. Fukuda, W.T. Elam, and R.L. Park, *Nitrogen, Oxygen, and Carbon Monoxide Chemisorption.* Applications of Surface Science **1**(1978) 278-287.

21. M.A. Omar, *Elementary Solid State Physics: Principles and Applications*. 1993.

22. K.S. Novoselov, A.K. Geim, S.V. Morozov, D. Jiang, M.I. Katsnelson, I.V. Grigorieva, S.V. Dubonos, and A.A. Firsov, *Two-dimensional gas of massless Dirac fermions in graphene.* Nature **438**(2005) 197-200.

23. J.S. Garitaonandia, M. Insausti, E. Goikolea, M. Suzuki, J.D. Cashion, N. Kawamura, H. Ohsawa, I.G.d. Muro, K. Suzuki, F. Plazaola, and T. Rojo, *Chemically induced permanent magnetism in Au, Ag, and Cu nanoparticles: Localization of the magnetism by element selective techniques.* Nano Letters **8**(2008) 661-667.

24. Y. Wang, Y.G. Nie, J.S. Pan, L. Pan, Z. Sun, and C.Q. Sun, *Layer and orientation resolved bond relaxation and quantum entrapment of charge and energy at Be surfaces.* Physical Chemistry Chemical Physics **12**(2010) 12753-9.

25. C.Q. Sun, Y. Nie, J. Pan, X. Zhang, S.Z. Ma, Y. Wang, and W. Zheng, *Zone-selective photoelectronic measurements of the local bonding and electronic dynamics associated with the monolayer skin and point defects of graphite.* Rsc Advances **2**(2012) 2377.

26. S.N. Frank and A.J. Bard, *Heterogeneous photocatalytic oxidation of cyanide and sulfite in aqueous solutions at semiconductor powders.* The Journal of Physical Chemlstry **81**(1977) 1484-1488.

27. M.V.Kuznetsov, A.V.Tel'minov, E.V.Shalaeva, and A.L.Ivanovskii, *Study of Adsorption of Nitrogen Monoxide on the Ti(0001) Surface.* The Physics of Metals and Metallography **89**(2000) 569-580.

28. Y. Wang, Y. Nie, L. Wang, and C.Q. Sun, *Atomic-layer- and crystal-orientation-resolved $3d_{5/2}$ binding energy shift of Ru(0001) and Ru(10-10) surfaces.* J. Phys. Chem. C **114**(2010) 5.

29. W. Gopel, J.A. Anderson, D. Frankel, M. Jaehnig, K. Phillips, J.A. Schafer, and G. Rocker, *Surface defects of $TiO_2(110)$: A combined XPS, XAES and ELS study.* Surface Science **139**(1984) 333-346.

30. C. Kittel, *Introduction to Solid State Physics 7th edn*. 1996.

31. C.Q. Sun, Y. Wang, Y.G. Nie, B.R. Mehta, M. Khanuja, S.M. Shivaprasad, Y. Sun, J.S. Pan, L.K. Pan, and Z. Sun, *Interface charge polarization and quantum trapping in AgPd and CuPd bimetallic alloy catalysts.* PCCP **12**(2010) 3131 - 3135